Mediterranean Journal of Pharmacy & Pharmaceutical Sciences
ISSN: 2789-1895 online
www.ppj.org.ly
doi: 10.5281/zenodo.24089805
ISSN: 2958-3101 print

ORIGINAL RESEARCH article

Conformational preferences, electronic properties, and predicted ADME profiles of N-cyclohexyl secondary enamines: A DFT and SwissADME study

Abdalhamid Alarafi [1], **Sali Ahmed** [2], **Raghad AbdulFatah** [1], and **Haneen A. Wali** [3 *]

[1] Department of Chemistry, Faculty of Arts and Sciences, University of Benghazi, Al-Abyar, Libya
[2] Department of Chemistry, Faculty of Arts and Sciences, University of Benghazi, Qaminis, Libya
[3] Libyan Center for Studies and Research of Environmental Science and Technology, Sabratha, Libya
[*] Author to whom correspondence should be addressed

Received: 27-08-2026, **Accepted:** 08-11-2026, **Published online:** 10-11-2026

Copyright© 2026. This open-access article is distributed under the *Creative Commons Attribution License*, which permits unrestricted use, distribution, and reproduction in any medium, provided the original work is properly cited.

HOW TO CITE THIS

Alarafi A, et al. Conformational preferences, electronic properties, and predicted ADME profiles of N-cyclohexyl secondary enamines: A DFT and SwissADME study. Mediterr J Pharm Pharm Sci. 2026; 6(4): 91-103. [Article number: 274]. https://doi.org/10.5281/zenodo.24089805

Keywords: Density functional theory, pharmacokinetic prediction, N-cyclohexyl secondary enamines

Abstract: The structural diversity of secondary enamines provides an opportunity to examine how substituent variation affects molecular conformation, electronic characteristics, and physicochemical behavior. In this study, four N-cyclohexyl secondary enamine derivatives were investigated using density functional theory at the B3LYP/6-31G level, complemented by SwissADME predictions. The computational investigation encompassed conformational analysis, vibrational frequencies, frontier molecular orbitals, global reactivity descriptors, and Mulliken atomic charges. Among the four optimized structures considered for each derivative, the Chair-Z structure exhibited the lowest calculated Gibbs free energy for all four compounds. Physicochemical properties, lipophilicity, aqueous solubility, pharmacokinetic profiles, and medicinal chemistry filters were also assessed. The derivatives showed molecular weights of 181.27-243.34 g/mol, topological polar surface areas of 29.10-38.33 Å², and three to five rotatable bonds. Their consensus Log P values ranged from 2.35 to 3.26, indicating moderate lipophilicity. Compound 3 consistently exhibited the most favorable predicted aqueous solubility, whereas the phenyl-containing compound 2 showed the lowest solubility across the three prediction models. All compounds satisfied Lipinski's rule of five and were computationally predicted to exhibit high gastrointestinal absorption and potential blood-brain barrier permeation, with no predicted P-glycoprotein substrate behavior. Compound 2 was distinguished by predicted inhibition of CYP1A2, CYP2C19, and CYP2D6. No PAINS alerts were detected, although a shared Michael-acceptor Brenk alert indicated a structural feature requiring further assessment. Mulliken analysis revealed a conserved polarization pattern within the enamine framework, with negatively charged nitrogen atoms and contrasting charges at the selected carbon sites. Overall, the study identifies substitution-dependent differences in predicted molecular behavior and provides a basis for experimental investigations of chemical reactivity, solubility, permeability, and metabolic interactions.

Introduction

Enamines are established intermediates in organic synthesis, particularly in transformations involving carbon–carbon bond formation. Their synthetic importance was demonstrated by Stork and co-workers through the alkylation and acylation of carbonyl compounds using enamine intermediates [1]. Their characteristic behavior arises from conjugation between the nitrogen lone pair and the adjacent carbon-carbon double bond. In carbonyl-conjugated secondary enamines, the additional carbonyl functionality creates a framework in

which molecular geometry and electronic polarization can be examined together. Such compounds provide a useful basis for investigating how structural modification affects molecular properties within a related series. The present derivatives share an N-cyclohexyl group while differing in the substituent associated with the carbonyl fragment. This arrangement allows comparison of ester, alkyl ketone, aryl ketone, and fluorinated ketone derivatives within a common molecular framework. Their characterization requires consideration of both the cyclohexyl ring conformation and the geometry of the conjugated enamine fragment. The relative orientation of the N-H and carbonyl groups is also relevant when assessing possible intramolecular interactions. Comparing these structural features can help distinguish changes associated with molecular conformation from those associated with substitution. Density functional theory provides a framework for investigating these questions through calculations of molecular geometries, energies, and electronic properties. The B3LYP approach incorporates the hybrid exchange formulation associated with Becke's work and the correlation functional developed [2, 3]. Applying the same computational method to all members of a series enables systematic comparison of their calculated properties. Geometry optimization and vibrational analysis can therefore be complemented by an examination of frontier molecular orbitals and electronic descriptors to develop a more complete molecular interpretation.

Global reactivity descriptors offer a quantitative perspective on differences in electronic behavior. Thus, the electrophilicity index introduced by Parr and others [4] combines electronic chemical potential and chemical hardness to characterize the energetic response associated with electron acceptance. Atomic population analysis provides a complementary local description. Mulliken's approach partitions the electronic population among atomic contributions, allowing charge distributions within the molecular framework to be examined [5]. In the present compounds, comparing the nitrogen atom and selected carbon sites can help describe polarization within the conjugated core. These descriptors should nevertheless be interpreted together with molecular geometry and orbital distributions rather than used independently to establish reaction pathways.

Physicochemical characterization addresses another aspect of molecular behavior relevant to subsequent biological investigation. Lipinski and co-workers established widely used relationships between molecular weight, lipophilicity, hydrogen-bonding capacity, and the likelihood of poor absorption or permeation [6]. Veber and colleagues subsequently demonstrated the importance of molecular flexibility and polar surface area in an experimental dataset of drug candidates [7]. These studies support the combined assessment of several molecular descriptors. They also show why compliance with an individual threshold should be treated as screening information rather than evidence of adequate oral exposure. Aqueous solubility deserves particular attention because structural changes that alter lipophilicity may also affect the amount of compound available in solution. Delaney's ESOL model provides a structure-based method for estimating aqueous solubility and illustrates the value of molecular descriptors in preliminary compound assessment [8]. Such estimates are useful for comparing related derivatives, although their numerical values remain predictions. Considering agreement and disagreement between different solubility models can help identify compounds for which experimental measurements are especially important.

SwissADME integrates physicochemical calculations, solubility estimates, pharmacokinetic predictions, and medicinal chemistry filters within a single platform [9]. Its outputs support comparison of gastrointestinal absorption, blood-brain barrier (BBB) permeability, P-glycoprotein substrate behavior, and inhibition of selected cytochrome P450 (CYP) isoforms. The BOILED-Egg model further illustrates how lipophilicity and polarity can be combined to estimate passive gastrointestinal absorption and brain penetration [10]. These predictions provide useful starting points for experimental planning, but they do not directly establish systemic exposure, metabolic stability, or biological efficacy. Structural alerts offer a further screening perspective. The PAINS filters developed by Baell and Holloway identify substructural features associated with frequent activity across biochemical screening assays [11]. Their application can highlight potential assay interference, while other medicinal chemistry filters flag structural features requiring additional investigation. An absence

of alerts should therefore be interpreted within the scope of the corresponding filter and should not be regarded as proof of safety or target specificity. Against this background, the present study combines B3LYP/6-31G calculations with SwissADME screening to characterize four N-cyclohexyl secondary enamine derivatives. The investigation examines conformational preferences, vibrational characteristics, frontier molecular orbitals, global reactivity descriptors, and atomic charge distributions, alongside predicted physicochemical and pharmacokinetic properties. The objective is to identify features conserved across the series and differences associated with carbonyl substitution, providing a basis for subsequent experimental evaluation of chemical reactivity, solubility, permeability, and metabolic interactions.

Materials and methods

SwissADME-based physicochemical and pharmacokinetic predictions: Drug-likeness and pharmacokinetic properties are commonly evaluated during the early stages of drug discovery and development. These assessments provide preliminary information about the physicochemical characteristics and ADME profiles of compounds, helping researchers prioritize candidates for further experimental investigation. SwissADME is a freely available web-based tool used to predict the physicochemical properties, lipophilicity, aqueous solubility, pharmacokinetic profiles, drug-likeness, and medicinal chemistry properties of small molecules [9]. The two-dimensional structures of compounds C1–C4 were drawn using ChemDraw 2023, and their corresponding SMILES representations (**Table 1**) were submitted to SwissADME for prediction and analysis. The Z-configured SMILES representation of each derivative was selected for SwissADME predictions based on the DFT results, which identified the Chair-Z structure as the lowest Gibbs free-energy geometry among the four candidate structures. It should be noted that the SMILES notation specifies the molecular connectivity and E/Z configuration but does not explicitly represent the cyclohexyl chair or boat conformation.

Key physicochemical parameters, including molecular weight (MW), number of heavy atoms (nHA), number of hydrogen bond donors (nHBD), number of hydrogen bond acceptors (nHBA), topological polar surface area (TPSA), molar refractivity (MR), fraction of sp^3 carbon atoms (Fsp^3), number of rotatable bonds (nRB), and aromatic heavy atoms (nAHA) were analyzed. Lipophilicity was assessed using the consensus LogP (log Po/w) model, while aqueous solubility was predicted using ESOL, Ali, and SILICOS-IT models. Drug-likeness was assessed using Lipinski's rule of five and the Ghose, Veber, Egan, and Muegge filters. Lead-likeness was also evaluated, and synthetic accessibility scores were recorded. Pharmacokinetic predictions included gastrointestinal absorption, BBB permeation, P-glycoprotein substrate status, and inhibition of selected CYP isoforms. Medicinal chemistry alerts were assessed using the PAINS and Brenk filters.

Table 1: SMILES notation of secondary enamine derivatives (C1–C4)

Compound	Z-Isomer SMILES Notation
C1	C/C(NC1CCCCC1)=C/C(OCC)=O
C2	C/C(NC1CCCCC1)=C/C(C2=CC=CC=C2)=O
C3	CC(/C=C(NC1CCCCC1)/C)=O
C4	C/C(NC1CCCCC1)=C/C(C(F)(F)F)=O

Computational methodology: All quantum chemical calculations were performed using Density Functional Theory (DFT) as implemented in the Gaussian 09 program package. GaussView was used to visualize molecular structures, frontier molecular orbitals (FMOs), vibrational spectra, and atomic charge distributions. All molecular systems were treated as neutral singlet species (total charge = 0; spin multiplicity = 1). For each derivative (Compounds C1-C4), four initial molecular structures were constructed manually using GaussView, representing the combinations of two geometrical configurations (E and Z) and two cyclohexyl ring conformations (chair and boat): Chair-Z, Chair-E, Boat-Z, and Boat-E. Here, E/Z refers to the geometric isomerism of the C=C double bond, whereas chair/boat refers to the conformational arrangement of the

cyclohexyl ring. Each geometry was then optimized independently in the gas phase using Gaussian 09 at the B3LYP/6-31G level of theory. The B3LYP functional combines Becke's three-parameter hybrid exchange functional with the Lee-Yang-Parr correlation functional. Harmonic vibrational frequency calculations were performed at the same level of theory to verify that each optimized geometry corresponds to a local minimum on the potential-energy surface, as indicated by the absence of imaginary frequencies (Nimag=0). Thermochemical corrections were evaluated at 298.15 K and 1 atm.

The unscaled harmonic vibrational frequencies were multiplied by a scaling factor of 0.9613, corresponding to the B3LYP/6-31G level of theory, to account for systematic deviations associated with the harmonic approximation and the computational method [12-14]. The calculated orbital energies were converted from Hartree to electronvolts (eV) using the conversion factor 1 Hartree=27.2114 eV. Gibbs free-energy differences were converted from Hartree to kcal mol^{-1} using the conversion factor 1 Hartree = 627.5095 kcal mol^{-1} before Boltzmann population calculations. The relative Boltzmann populations (P_i) of the four optimized structures (Chair-Z, Chair-E, Boat-Z, and Boat-E) were estimated at T=298.15 K based on their relative Gibbs free energies (ΔG_i) using a single Boltzmann distribution. This approach assumes thermodynamic equilibrium among all four structures. Therefore, the calculated populations represent theoretical equilibrium estimates rather than experimentally measured isomeric compositions.

$$P_i = \frac{\exp\left(-\frac{\Delta G_i}{RT}\right)}{\sum_j \exp\left(-\frac{\Delta G_j}{RT}\right)} \times 100\%$$

Here, ΔG_i represents the Gibbs free energy of optimized structure i relative to the lowest-energy structure. R is the universal gas constant (1.9872×10^{-3} kcal mol^{-1} K^{-1}), and T is the absolute temperature (298.15 K). The summation in the denominator includes all four optimized structures: Chair-Z, Chair-E, Boat-Z, and Boat-E. Global reactivity descriptors were evaluated based on Conceptual DFT (CDFT) under Koopmans' approximation using the calculated energies of the Highest Occupied Molecular Orbital (E_{HOMO}) and Lowest Unoccupied Molecular Orbital (E_{LUMO}):

Energy gap: $\Delta E_{\mathrm{gap}} = E_{\mathrm{LUMO}} - E_{\mathrm{HOMO}}$, **Ionization potential:** $I = -E_{\mathrm{HOMO}}$, **Electron affinity:** $A = -E_{\mathrm{LUMO}}$, **Chemical hardness:** $\eta = \frac{I-A}{2}$, **Chemical softness:** $S = \frac{1}{2\eta}$, **Electronegativity:** $\chi = \frac{I+A}{2}$, **Chemical potential:** $\mu = -\chi$, **Global electrophilicity index:** $\omega = \frac{\mu^2}{2\eta}$, and **Global nucleophilicity index:** $N = E_{\mathrm{HOMO}} - E_{\mathrm{HOMO(TCE)}}$, where $E_{\mathrm{HOMO(TCE)}} = -8.6559$ eV

The HOMO energy of TCE (-8.6559 eV), calculated at the DFT/B3LYP/6-31G level, was adopted as the reference value, as reported by Khelfaoui et al. [15].

Mulliken population analysis was performed using the Gaussian 09 output files for the optimized global-minimum (Chair-Z) structures of compounds C1-C4. The atomic charge distributions were analyzed to characterize the electronic polarization within the enamine framework, with particular attention to four selected sites: the enamine nitrogen (N), α-carbon (Cα), β-carbon (Cβ), and N–H hydrogen atom.

Results and discussion

Analysis of physicochemical properties: The physicochemical properties of the four N-cyclohexyl secondary enamine derivatives (C1-C4) were evaluated using SwissADME, and the predicted results are summarized in **Table 2**. The molecular weights ranged from 181.27 to 243.34 g/mol, indicating relatively low molecular masses across the investigated series. Compound C3 exhibited the lowest molecular weight (181.27 g/mol), whereas C2 showed the highest value (243.34 g/mol), reflecting the contribution of its additional phenyl substituent.

Table 2: Predicted physicochemical properties of the secondary enamine derivatives (C1-C4) calculated using SwissADME

Compound	MW (g/mol)	nHA	nAHA	F.sp3	nRB	nHBA	nHBD	MR	TPSA(Å²)
C1	211.30	15	0	0.75	5	2	1	61.30	38.33
C2	243.34	18	6	0.44	4	1	1	75.31	29.10
C3	181.27	13	0	0.73	3	1	1	55.40	29.10
C4	235.25	16	0	0.73	4	4	1	55.60	29.10

The fraction of sp³-hybridized carbon atoms (Fsp³) ranged from 0.44 to 0.75. Compound C2 displayed the lowest Fsp³ value (0.44), consistent with its aromatic phenyl group, while C1, C3, and C4 exhibited higher values (0.73-0.75), indicating a greater proportion of saturated carbon atoms. The number of rotatable bonds varied between three and five, with C3 showing the lowest value (3), suggesting relatively limited conformational flexibility. In addition, all four compounds possessed one hydrogen-bond donor, while the predicted hydrogen-bond acceptor counts ranged from one to four. The topological polar surface area (TPSA) values were relatively low, ranging from 29.10 to 38.33 Å². Compound C1 exhibited the highest TPSA (38.33 Å²), whereas the remaining compounds showed identical values of 29.10 Å². Molar refractivity values ranged from 55.40 to 75.31, with C2 exhibiting the highest value. Overall, the predicted physicochemical descriptors indicate that the four derivatives share relatively low molecular weights, limited molecular flexibility, and low polar surface areas. These characteristics may be favorable for passive membrane permeability, although experimental studies would be required to confirm their actual permeability behavior.

Lipophilicity and water solubility: The consensus Log P values ranged from 2.28 to 3.44, indicating moderate lipophilicity across the investigated series. Compound C2 exhibited the highest lipophilicity (3.44), whereas C3 showed the lowest value (2.28). Regarding aqueous solubility, C3 consistently displayed the most favorable predictions across the ESOL, Ali, and SILICOS-IT models, while C2 showed the lowest predicted solubility. This trend suggests that the additional aromatic ring in C2 may contribute to its higher lipophilicity and comparatively reduced aqueous solubility. Despite differences in the numerical estimates, the three models showed consistent trends across the series, highlighting C2 as a compound requiring particular attention in experimental solubility assessment (**Table 3**).

Table 3: Predicted lipophilicity and aqueous solubility of the secondary enamine derivatives (C1–C4) calculated using SwissADME

Compound	Lipophilicity	Water solubility					
	Consensus Log Po/w	Log S (ESOL)	Solubility Class	Log S (All)	Solubility Class	Log S (SILICOS-IT)	Solubility Class
1	2.57	-2.99	Soluble	-3.93	Soluble	-2.33	Soluble
2	3.44	-4.21	Moderately soluble	-4.90	Moderately soluble	-4.32	Moderately soluble
3	2.28	-2.60	Soluble	-3.18	Soluble	-2.18	Soluble
4	3.06	-3.57	Soluble	-4.33	Soluble	-2.69	Soluble

Pharmacokinetic profile: All derivatives were predicted to exhibit high gastrointestinal absorption and BBB permeability, while none was classified as a P-glycoprotein substrate. The principal difference concerned CYP inhibition: Compound 2 was predicted to inhibit CYP1A2, CYP2C19, and CYP2D6, whereas compounds 1, 3, and 4 showed no predicted inhibition of the five evaluated isoforms. Compound 2 therefore warrants closer investigation for potential metabolic interactions. These classifications remain computational predictions and do not establish oral bioavailability, brain exposure, or clinical interaction risk (**Table 4**).

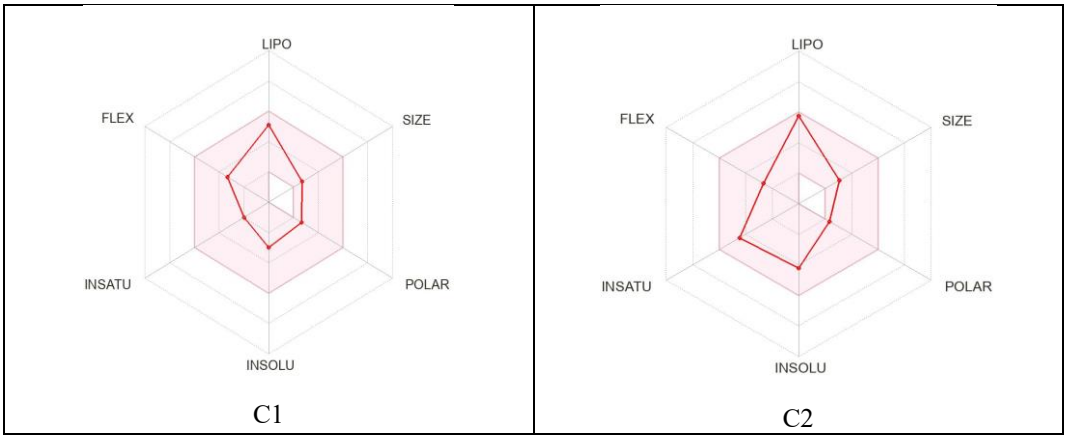
Table 4: Predicted pharmacokinetic profiles of the secondary enamine derivatives (C1-C4) calculated using SwissADME

Compound	GI absorption	BBB permeant	P-gp substrate	CYP1A2 inhibitors	CYP2C19 inhibitors	CYP2C9 inhibitors	CYP2D6 inhibitors	CYP3A4 inhibitors
1	High	Yes	No	No	No	No	No	No
2	High	Yes	No	Yes	Yes	No	Yes	No
3	High	Yes	No	No	No	No	No	No
4	High	Yes	No	No	No	No	No	No

Drug likeness and medicinal chemistry: All four compounds satisfied Lipinski, Ghose, Veber, and Egan criteria, indicating favorable predicted drug-likeness profiles according to these filters. However, compound C3 failed the Muegge filter because its molecular weight was below 200 g/mol. None of the derivatives met the lead-likeness criteria, primarily due to their molecular weights being below the specified range, with additional XLOGP3 violations observed for C2 and C4 (**Figure 1**). Although no PAINS alerts were detected, all compounds exhibited a common Michael-acceptor Brenk alert, indicating a structural feature that warrants further investigation of their chemical reactivity. The synthetic accessibility scores (2.64-2.95) suggest relatively accessible molecular structures, although experimental synthesis is required to establish their actual synthetic feasibility (**Table 5, Figure 2**).

Table 5: Drug-likeness assessment and medicinal chemistry profiles of the secondary enamine derivatives (C1–C4) evaluated using SwissADME

Compound	Drug-likeness rules					Medicinal chemistry			
	Lipinski	Ghose	Veber	Egan	Muegge	PAINS	Brenk	Lead likeness	Synthetic accessibility
1	Yes; 0 violations	Yes	Yes	Yes	Yes	0 alert	1 alert: michael_acceptor_1	No; 1 violation: MW<250	2.70
2	Yes; 0 violations	Yes	Yes	Yes	Yes	0 alert	1 alert: michael_acceptor_1	No; 2 violations: MW<250, XLOGP3>3.5	2.64
3	Yes; 0 violations	Yes	Yes	Yes	No; 1 violation: MW<200	0 alert	1 alert: michael_acceptor_1	No; 1 violation: MW<250	2.67
4	Yes; 0 violations	Yes	Yes	Yes	Yes	0 alert	1 alert: michael_acceptor_1	No; 2 violations: MW<250, XLOGP3>3.5	2.95



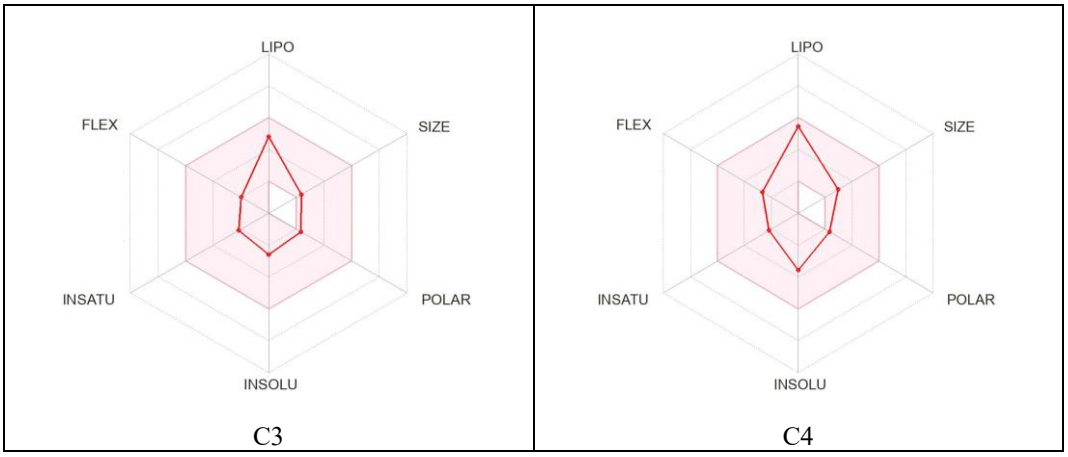


Figure 1: Radar chart illustrating the physicochemical properties and drug-likeness descriptors of the secondary enamine derivatives (C1-C4)

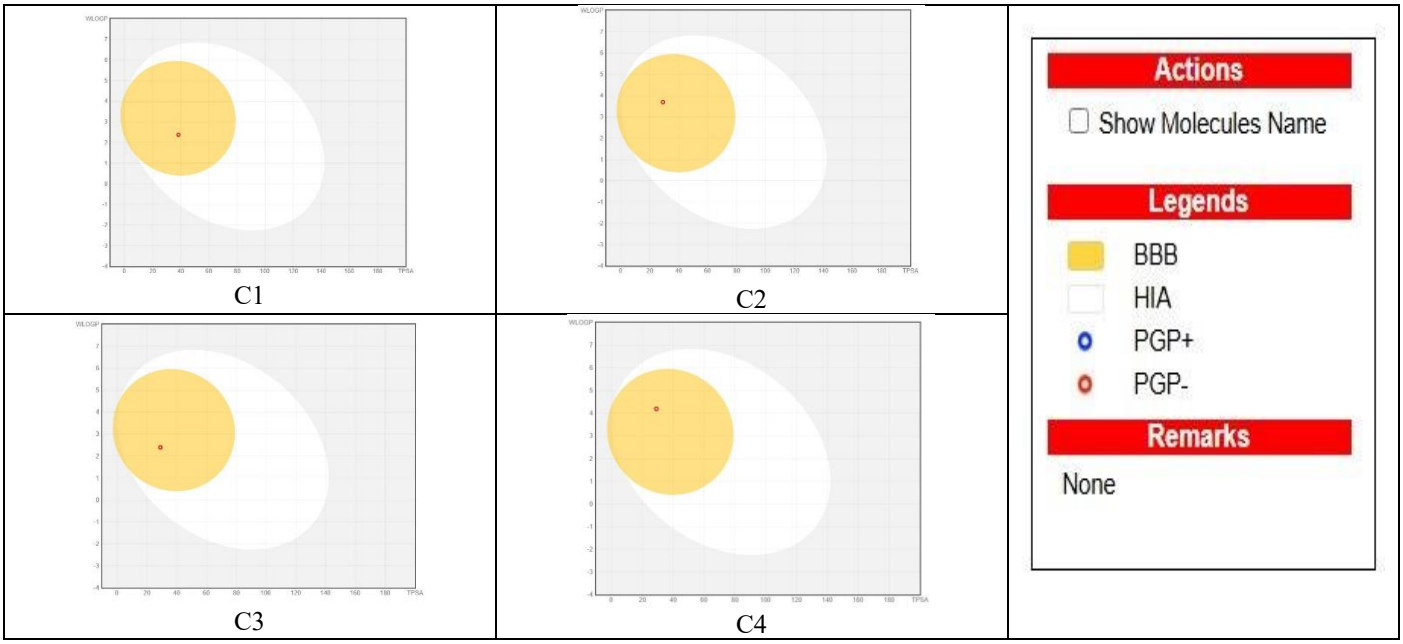


Figure 2: BOILED-Egg plot of the secondary enamine derivatives (C1–C4) showing predicted gastrointestinal absorption and blood-brain barrier permeability, along with P-glycoprotein substrate status.

DFT simulation: A comparative conformational analysis was performed for compounds C1-C4 by considering four structural arrangements resulting from the combination of E/Z geometric isomerism and chair/boat conformations of the cyclohexyl ring. We used the Gibbs free energies from the Gaussian calculations to assess the relative thermodynamic stability of these conformers and estimate their equilibrium populations at 298.15 K (**Figure 3**).

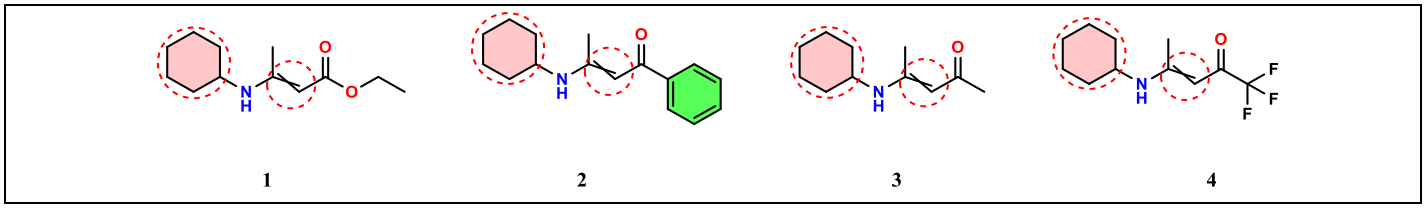


Figure 3: 2D Chemical structures of the studied cyclohexane-based secondary enamine derivatives (compounds 1- 4).

As shown in **Table 6**, the Chair-Z conformer was the lowest-energy structure for all four compounds. However, the extent of this preference varied among the derivatives. The Gibbs free-energy differences between the Chair-Z and Chair-E conformers were 5.002, 2.003, 1.350, and 2.303 kcal mol^{-1} for C1, C2, C3, and C4, respectively. The corresponding Boltzmann populations of the Chair-Z conformer were 99.97%,

96.71%, 90.71%, and 97.98%, respectively. These results indicate that C1 exhibits the strongest conformational preference for the Chair-Z arrangement, whereas C3 shows a comparatively smaller energetic separation between its two chair conformers. The relatively higher contribution of Chair-E in C3 suggests that its conformational distribution is more sensitive to the structural features of the substituent attached to the carbonyl-containing fragment. In addition, both boat conformers exhibit higher Gibbs free energies than the corresponding chair conformers, indicating a consistent thermodynamic preference for the chair arrangement across the investigated series (**Figure 4**).

Table 6: Thermodynamic energies and relative stability of the enamine derivatives across all studied conformers at B3LYP/6-31G ($T = 298.15$ K)

Compound	Conformer	Electronic Energy (E_{elec}, Hartree)	Zero-Point Energy (ZPE, Hartree)	Total Free Energy (G, Hartree	ΔG (kcal/mol)	Population (P_i, %)
1	Chair-Z Chair-E Boat-Z Boat-E	674.963838- 674.954269- 674.953496- 674.943933-	0.323738 0.323194 0.323529 0.323121	674.684632- 674.676661- 674.675951- 674.667149-	0.000 5.002 + 5.447 + 10.971+	99.9683 0.0216 0.0102 0.0000
2	Chair-Z Chair-E Boat-Z Boat-E	752.138359- 752.135408- 752.127935- 752.124985-	0.343779 0.343645 0.343834 0.343482	751.840743- 751.837551- 751.830773- 751.828460-	0.000 2.003+ 6.256+ 7.708+	96.7069 3.2903 0.0025 0.0002
3	Chair-Z Chair-E Boat-Z Boat-E	560.442735- 560.439489- 560.432343- 560.429208-	0.290149 0.289679 0.289825 0.289805	560.193397- 560.191245- 560.184542- 560.181443-	0.000 1.350+ 5.557+ 7.501+	90.7069 9.2852 0.0077 0.0003
4	Chair-Z Chair-E Boat-Z Boat-E	858.088796- 858.084065- 858.078782- 858.073835-	0.266323 0.265947 0.266239 0.266072	857.866779- 857.863109- 857.857731- 857.852872-	0.000 2.303+ 5.678+ 8.727+	97.9838 2.0094 0.0068 0.0000

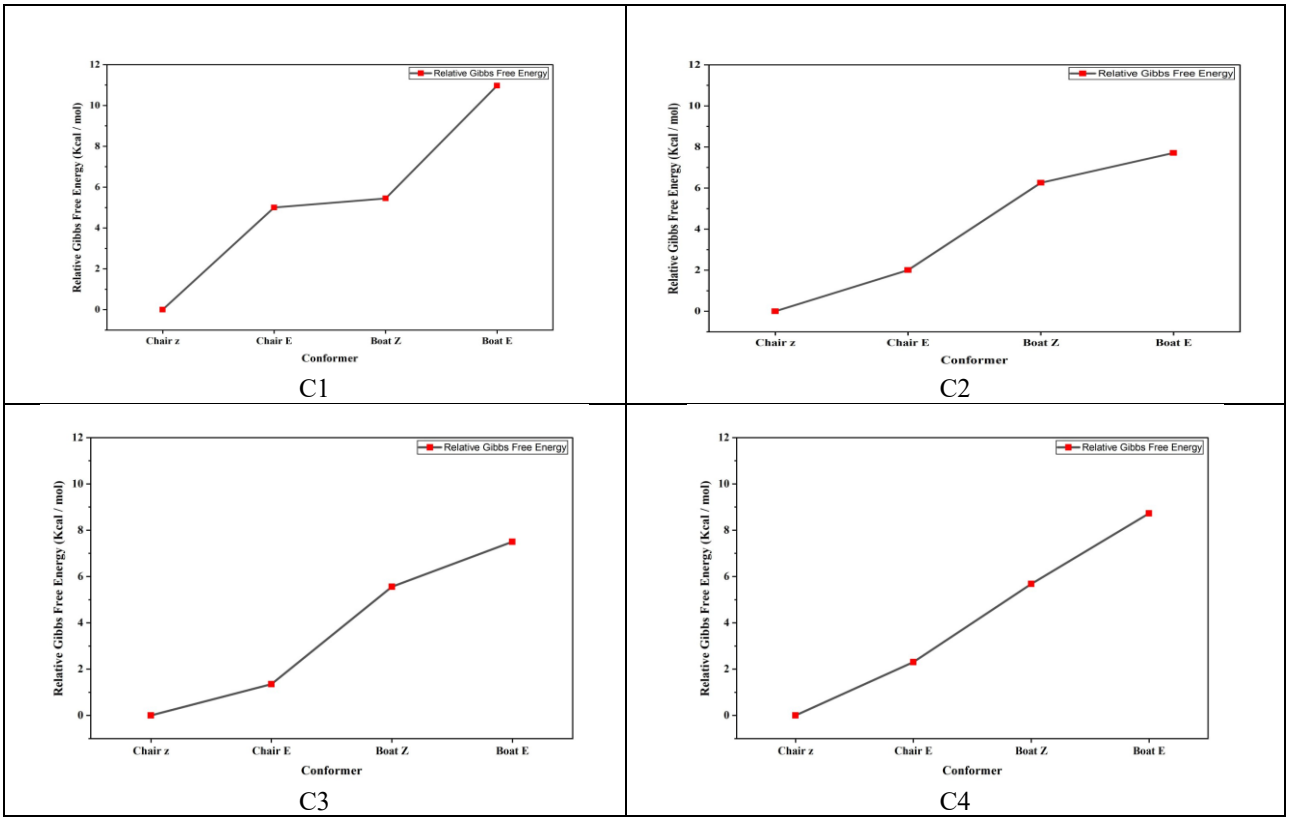


Figure 4: Relative energy profiles of the four conformers (Chair-Z, Chair-E, Boat-Z, and Boat-E) for compounds C1–C4

Vibrational frequency analysis (FT-IR): The calculated N–H stretching frequencies of the Chair-Z conformers of compounds C1–C4 are presented in **Table 7**. The unscaled frequencies range from 3506.82 to 3652.74 cm^{-1}, while the corresponding scaled values, obtained using a scaling factor of 0.9613, fall within the range of 3371.11–3511.38 cm^{-1}. A clear variation in the N–H stretching frequency is observed across the investigated compounds. Compound C1 exhibits the lowest scaled frequency (3371.11 cm^{-1}), whereas C3 displays the highest value (3511.38 cm^{-1}). Compounds C2 and C4 show intermediate frequencies of 3460.84 and 3475.10 cm^{-1}, respectively. This variation indicates that the vibrational environment of the N–H bond is sensitive to changes in the molecular structure and the nature of the attached substituents. The relatively lower N–H stretching frequency calculated for C1 may reflect a greater perturbation of the N–H bond compared with the other derivatives. Such a shift can potentially arise from differences in intramolecular interactions or local electronic effects. However, the frequency values alone are insufficient to establish the presence or strength of intramolecular hydrogen bonding. Additional structural parameters, particularly the N···O distance and N–H···O angle, are required to support such an interpretation. Overall, the observed differences in N–H stretching frequencies demonstrate that structural modifications across the investigated series influence the local vibrational characteristics of the enamine framework (**Figure 5**). These findings provide complementary evidence of substituent-dependent electronic and structural effects within compounds C1–C4.

Table 7: Calculated N–H Stretching Frequencies of the Chair-Z Conformers of Compounds C1–C4 at the B3LYP/6-31G Level

Compound	Unscaled ν_{N-H} (cm^{-1})	Scaledν_{N-H} (cm^{-1})*
1	3506.82	3371.11
2	3600.16	3460.84
3	3652.74	3511.38
4	3615.00	3475.10

*Scaled using 0.9613 factor

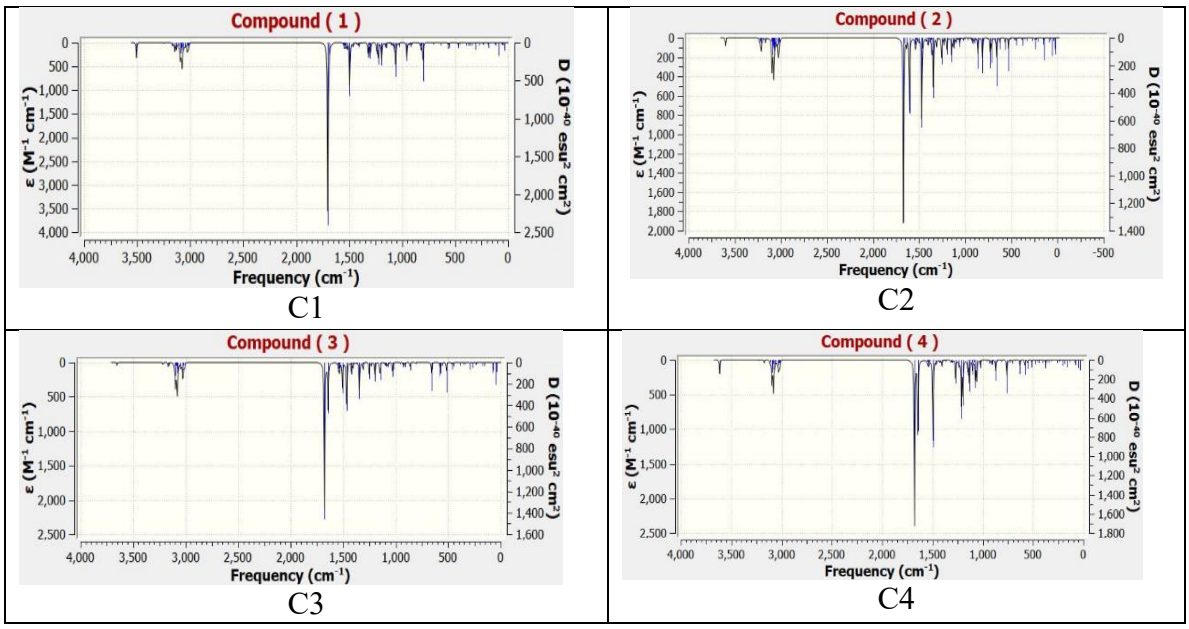
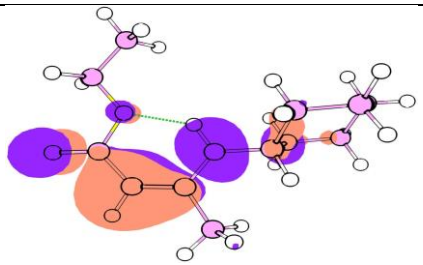
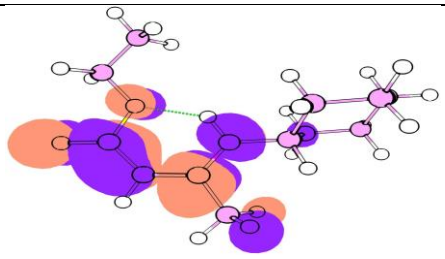
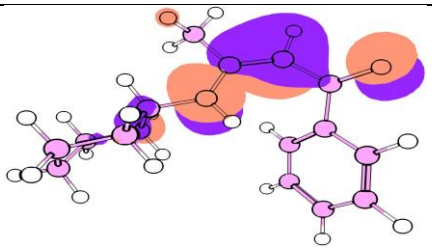
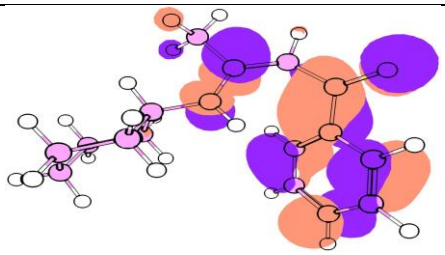
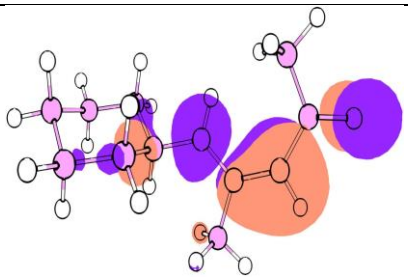
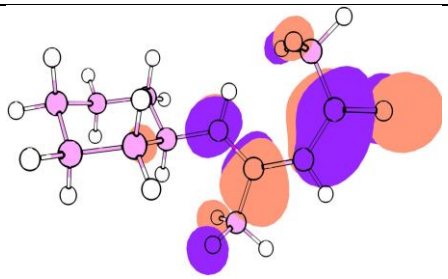
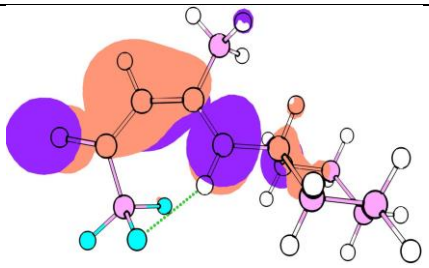
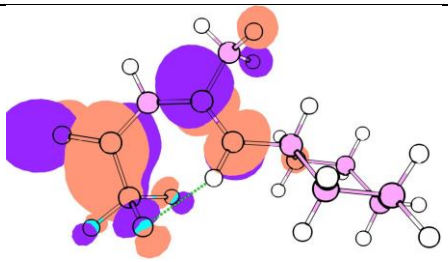


Figure 5: Calculated FT-IR spectra of compounds 1-4 at B3LYP/6-31G level of theory

Frontier Molecular Orbitals (FMO) and global reactivity descriptors: Frontier orbital spatial distributions show that the HOMO electron density is predominantly localized over the enamine C=C double bond and the nitrogen lone pair, whereas the LUMO density is shifted towards the conjugated electron-withdrawing carbonyl/aromatic regions (**Table 8**).

Table 8: Frontier Molecular Orbitals (HOMO and LUMO) distributions for the global minimum (Chair-Z) of Compounds 1–4

Compound	HOMO	LUMO
1		
2		
3		
4		

In **Table 9**, the electronic properties of compounds C1–C4 were investigated through frontier molecular orbital analysis and global reactivity descriptors. As presented in Table 9, the HOMO energies range from -5.3596 to -5.9998 eV, while the LUMO energies vary between -0.3459 and -1.7013 eV. Compound C1 exhibits the highest HOMO energy, whereas C4 possesses the lowest LUMO energy, indicating differences in the electronic characteristics of the investigated derivatives. The calculated HOMO-LUMO energy gaps follow the order C2 (4.2112 eV) < C4 (4.2985 eV) < C3 (4.8583 eV) < C1 (5.0137 eV). Accordingly, C2 exhibits the smallest energy gap and the highest chemical softness (0.2375 eV^{-1}), suggesting a comparatively greater tendency toward electronic density redistribution. In contrast, C1 displays the highest chemical hardness (2.5068 eV) and the lowest softness (0.1995 eV^{-1}).

Regarding the remaining global descriptors, C4 exhibits the highest electronegativity (3.8506 eV) and electrophilicity index (3.4492 eV), indicating the strongest predicted global electrophilic character within the series. Conversely, C1 shows the highest nucleophilicity index (3.2963 eV). These differences highlight the influence of structural substitution on the electronic characteristics of the investigated enamine derivatives. Overall, the combined FMO and global reactivity analyses reveal distinct electronic profiles among the four compounds. C2 is characterized by the smallest energy gap and highest softness; C4 exhibits the highest electrophilicity, while C1 displays the highest nucleophilicity and hardness. These complementary descriptors provide a comparative understanding of the electronic behavior of the investigated compounds.

Table 9: Global reactivity descriptors calculated at B3LYP/6-31G for the global minimum (Chair-*Z*) of compounds 1–4

Descriptor	Compound 1	Compound 2	Compound 3	Compound 4
E_{HOMO} (eV)	−5.3596	−5.3908	−5.4537	−5.9998
E_{LUMO} (eV)	−0.3459	−1.1796	−0.5954	−1.7013
ΔE_{gap} (eV)	5.0137	4.2112	4.8583	4.2985
Ionization Potential (I, eV)	5.3596	5.3908	5.4537	5.9998
Electron Affinity (A, eV)	0.3459	1.1796	0.5954	1.7013
Chemical Hardness (η, eV)	2.5068	2.1056	2.4292	2.1493
Chemical Softness (S, eV^{-1})	0.1995	0.2375	0.2058	0.2326
Electronegativity (χ, eV)	2.8527	3.2852	3.0245	3.8506
Chemical Potential (μ, eV)	−2.8527	−3.2852	−3.0245	−3.8506
Electrophilicity Index (ω, eV)	1.6231	2.5628	1.8829	3.4492
Nucleophilicity Index (N, eV)	3.2963	3.2651	3.2022	2.6561

Mulliken atomic charge distribution and local reactivity: Mulliken population analysis was performed to examine the electronic charge distribution within compounds C1–C4. As shown in **Table 10**, the enamine nitrogen exhibits a consistently negative charge (-0.691 to -0.702 e), reflecting its electron-rich character. In contrast, the α-carbon carries a positive charge (+0.388 to +0.409 e), whereas the β-carbon exhibits negative values (-0.224 to -0.233 e), indicating polarization across the enamine framework.

Among the investigated derivatives, C3 shows the most negative nitrogen charge (-0.702 e), while C4 exhibits the highest positive charge at the α-carbon (+0.409 e). C2 displays the most negative β-carbon charge (-0.233 e). The amine hydrogen remains positively charged in all compounds, with values ranging from +0.315 to +0.359 e, the highest being observed for C1. Overall, the results indicate that structural modifications influence the local charge distribution while preserving the characteristic electronic polarization of the enamine system (**Figure 6**). These findings complement the frontier molecular orbital analysis and provide further insight into the electronic characteristics of the investigated compounds [16, 17].

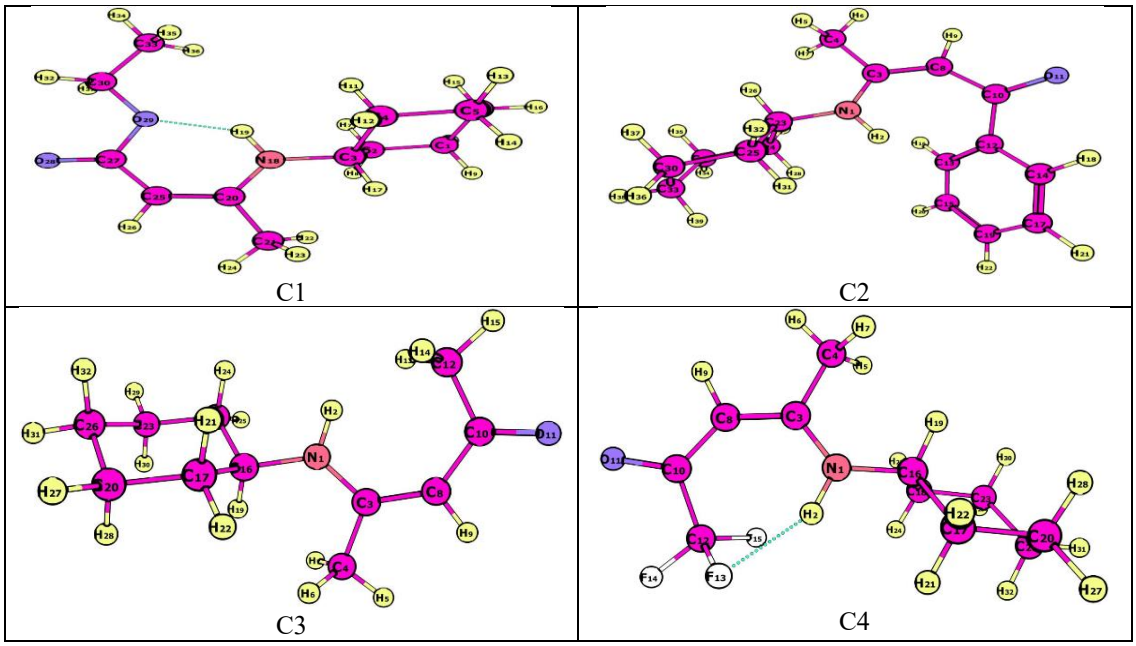


Figure 6: Optimized geometries with atomic numbering for the global minimum (Chair-Z) of Compounds 1–4

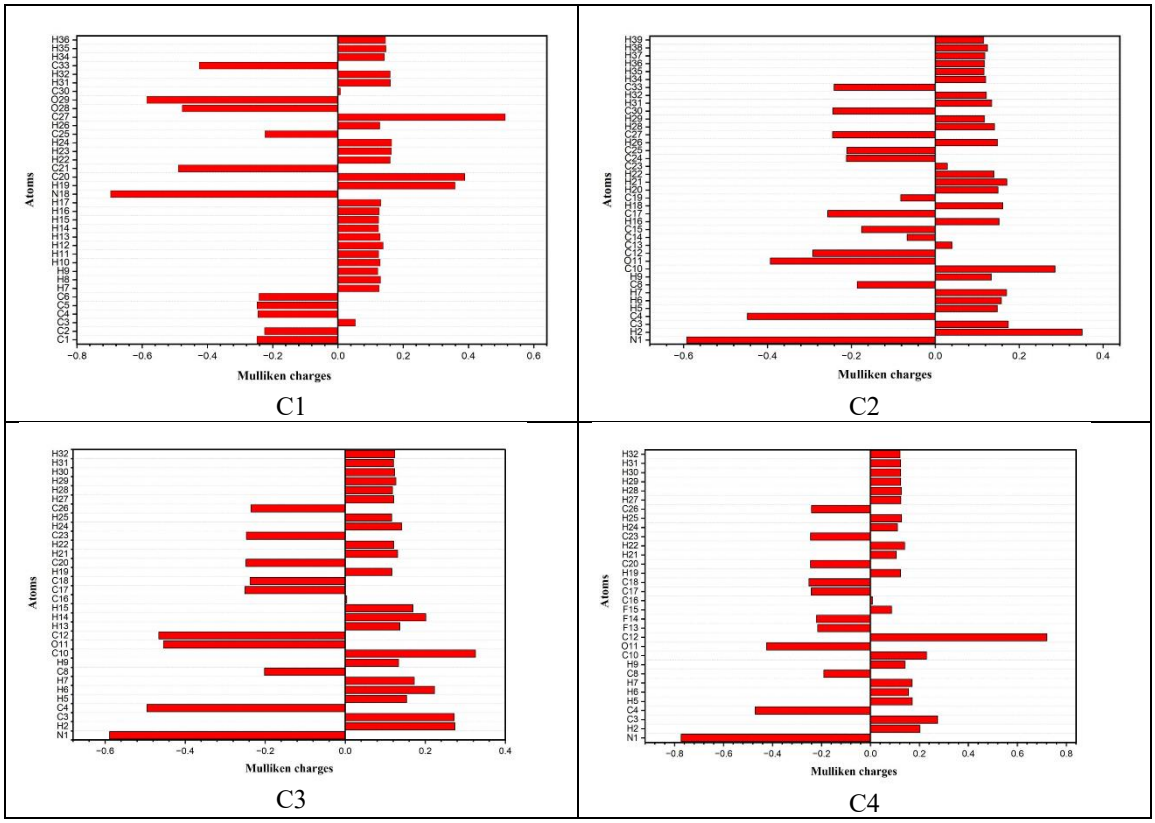


Figure 7: Mulliken atomic charge distribution of the secondary enamine derivatives (C1–C4)

Table 10: Selected Mulliken Atomic Charges (*e*) for the global minimum (Chair-*Z*) of Compounds 1–4

Atom/Site	Compound 1	Compound 2	Compound 3	Compound 4
Enamine nitrogen (N)	- 0.696	- 0.691	- 0.702	- 0.697
α-Carbon (C_α)	0.389	0.390	0.388	0.409
β-Carbon (C_β)	- 0.224	- 0.233	- 0.225	- 0.226
Amine hydrogen (H_{N-H})	0.359	0.323	0.315	0.341

Conclusion: This study combined density functional theory calculations at the B3LYP/6-31G level with SwissADME predictions to investigate the physicochemical, conformational, and electronic properties of four N-cyclohexyl secondary enamine derivatives (C1–C4). The predicted physicochemical properties revealed relatively low molecular weights (181.27-243.34 g/mol), low topological polar surface areas (29.10-38.33 Å²), and moderate lipophilicity, with consensus Log P values ranging from 2.28 to 3.44. Compound C3 exhibited the most favorable predicted aqueous solubility, whereas C2 showed the lowest solubility. All derivatives satisfied Lipinski's rule of five and were predicted to exhibit high gastrointestinal absorption and BBB permeability. However, C2 showed predicted inhibition of CYP1A2, CYP2C19, and CYP2D6, while all compounds displayed a common Michael-acceptor Brenk alert. Conformational analysis identified Chair-Z as the most stable conformer for all four derivatives. The vibrational analysis further provided information on the N–H stretching characteristics of the investigated compounds and supported the examination of their optimized molecular structures. The frontier molecular orbital analysis revealed notable differences in electronic properties. C2 exhibited the smallest HOMO–LUMO energy gap (4.2112 eV) and the highest chemical softness, whereas C4 showed the highest electronegativity and global electrophilicity. In contrast, C1 exhibited the highest nucleophilicity index. Mulliken population analysis demonstrated a consistent charge-polarization pattern across the enamine framework, with negatively charged nitrogen and β-carbon atoms and positively charged α-carbon and N–H hydrogen atoms. Overall, the results demonstrate that structural modifications influence the conformational, electronic, and predicted physicochemical characteristics of the investigated derivatives.

References

1. Stork G, Brizzolara A, Landesman H, Szmuszkovicz J, Terrell R. The enamine alkylation and acylation of carbonyl compounds. Journal of the American Chemical Society. 1963; 85(2): 207-222. doi: 10.1021/ja00885a021
2. Becke AD. Density-functional thermochemistry. III. The role of exact exchange. The Journal of Chemical Physics. 1993; 98(7): 5648-5652. doi: 10.1063/1.464913
3. Lee C, Yang W, Parr RG. Development of the Colle-Salvetti correlation-energy formula into a functional of the electron density. Physical Review B. 1988; 37(2): 785-789. doi: 10.1103/PhysRevB.37.785
4. Parr RG, von Szentpály L, Liu S. Electrophilicity index. Journal of the American Chemical Society. 1999; 121(9): 1922-1924. doi: 1021/ja983494x
5. Mulliken RS. Electronic population analysis on LCAO-MO molecular wave functions. I. The Journal of Chemical Physics. 1955; 23(10): 1833-1840. doi: 10.1063/1.1740588
6. Lipinski CA, Lombardo F, Dominy BW, Feeney PJ. Experimental and computational approaches to estimate solubility and permeability in drug discovery and development settings. Advanced Drug Delivery Reviews. 1997; 23(1-3): 3-25. doi: 10.1016/S0169-409X(96)00423-1
7. Veber DF, Johnson SR, Cheng H-Y, Smith BR, Ward KW, Kopple K. Molecular properties that influence the oral bioavailability of drug candidates. Journal of Medicinal Chemistry. 2002; 45(12): 2615-2623. doi: 10.1021/jm020017n
8. Delaney JS. ESOL: Estimating aqueous solubility directly from molecular structure. Journal of Chemical Information and Computer Sciences. 2004; 44(3): 1000-1005. doi: 10.1021/ci034243x
9. Daina A, Michielin O, Zoete V. SwissADME: A free web tool to evaluate pharmacokinetics, drug-likeness and medicinal chemistry friendliness of small molecules. Scientific Reports. 2017; 7: 42717. doi: 10.1038/srep427
10. Daina A, Zoete V. A BOILED-Egg to predict gastrointestinal absorption and brain penetration of small molecules. ChemMedChem. 2016; 11(11): 1117-1121. doi: 10.1002/cmdc.201600182
11. Baell JB, Holloway GA. New substructure filters for removal of pan assay interference compounds (PAINS) from screening libraries and for their exclusion in bioassays. Journal of Medicinal Chemistry. 2010; 53(7): 2719-2740. doi: 10.1021/jm901137j
12. Ahmad I, Kuznetsov AE. Pirzada AS, Alsharif KF, Daglia M, Khan H. Computational pharmacology and computational chemistry of 4-hydroxyisoleucine: Physicochemical, pharmacokinetic, and DFT-based approaches. Frontiers in Chemistry. 2023; 11: 1145974. doi: 10.3389/fchem.2023.1145974
13. National Institute of Standards and Technology. Computational Chemistry Comparison and Benchmark Database: Precomputed vibrational scaling factors (Standard Reference Database 101, Release 22), 2022.
14. Alharati SH, Gbaj HA, Gabj MA, Hermann A, Gbaj AM. Computational screening of natural small molecules as dual ATXN3 and LC3 binders for an autophagy-based strategy in spinocerebellar ataxia type 3. Mediterranean Journal of Medical Research. 2026; 3(1): 94-104. doi: 10.5281/zenodo.18945545
15. Khelfaoui H, Harkati D, Saleh BA. Molecular docking, molecular dynamics simulations and reactivity studies on an approved drug library targeting ACE2 and SARS-CoV-2 binding with ACE2. Journal of Biomolecular Structure and Dynamics. 2021; 39(18): 7246-7262. doi: 10.1080/07391102.2020.1803967
16. Oluwamodupe C, Adelabu MM, Balogun CO. Molecular docking of medicinal plants: Towards metabolic disease management. Mediterranean Journal of Medical Research. 2026; 3(3): 238-244. doi: 10.5281/zenodo.2203497921
17. Ieban NA, Gbaj HA, Gbaj MA, Hermann A, Gbaj AM. Immune profile score of modified Tremelimumab withCTLA-4 could enhance immunotherapy using molecular docking. Mediterranean Journal of Medicine and Medical Sciences. 2026; 2(1): 40-50. doi: 10.5281/zenodo.18667523
18. Okoh EU, Aiwonegbe AE. Screening of antimicrobial phytochemicals from *Allium sativum* against bacterial and fungal drug targets: Insights from molecular docking and ADMET analysis. Mediterranean Journal of Medical Research. 2026; 3(3): 289-300. doi: 10.5281/zenodo.22816383

Authors' contributions: AAA conceived and designed the study. AAA, SAA & RAA collected data. RAA contributed to data analysis. AAA & SAA performed and interpreted the data. HAW drafted the manuscript and revised the important intellectual context. ALL authors reviewed and approved the final version of the manuscript.
Conflict of interest: The authors declare the absence of any commercial or financial relationships that could be construed as a potential conflict of interest.
Author declarations: The authors fully observed ethical standards, including avoiding plagiarism, informed consent, data fabrication or falsification, and double publication or submission.
Data availability statement: The raw data that support the findings of this article are available from the corresponding author upon reasonable request.
Generative AI disclosure: During the preparation of this manuscript, the authors used an AI tool for language editing and grammatical correction.